THE JOURNAL OF PHYSICAL CHEMISTRY C

Article

pubs.acs.org/JPCC

Growth, Structure, and Vibrational Properties of Few Layer Graphene Grown on Rh(111)

K. D. Gibson and S. J. Sibener*

The James Franck Institute and Department of Chemistry, The University of Chicago, 929 E. 57th Street, Chicago, Illinois 60637, United States

ABSTRACT: We examine the growth of supported multilayer graphene overlayers on a Rh(111) single crystal substrate. At elevated surface temperatures, ethylene dissociates on the surface and carbon is absorbed into the bulk of the Rh. When the crystal is slowly cooled, the carbon diffuses to the surface and forms multilayer graphene films. The thickness was determined by Auger electron spectroscopy and the surface ordering by He scattering. The top layer is azimuthally aligned with the Rh(111) surface, and the moiré pattern due to the lattice mismatch between the Rh and graphite is still visible, though greatly attenuated, for thicknesses up to four layers. We also used He scattering to measure the low-energy vibrations of the surface for both monolayer and multilayer graphene. One set of experiments measured the thermal attenuation of the elastic He scattering. The result was that the monolayer graphene is much "stiffer" (a higher Debye temperature) than even ∼2 layers. We also used time- and angle-resolved inelastic He scattering to measure the low-energy modes near the zone center. Unlike the graphite ZA acoustic mode, which goes to zero frequency at the zone center, the monolayer has a mode that is a nearly constant 7 meV near the zone center. On the other hand, multilayer graphene has a mode that much more closely resembles the ZA mode of graphite. For the low-lying phonons with some degree of polarization perpendicular to the surface, our observations indicate that there is a real difference in the surface dynamical properties as one transitions between a supported two-dimensional monolayer to three-dimensional films consisting of only a few atomic layers in thickness. These findings add important information on how the properties of supported graphene films evolve with dimensional crossover from 2D to 3D systems, knowledge that is needed for achieving targeted properties in thin films of 2D materials.

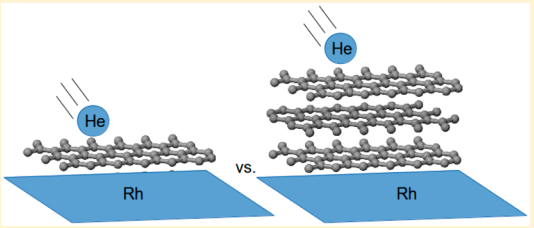

INTRODUCTION

There is intense interest in graphene, both single layers and multiple stacked layers, with each layer having sp^2-bonded C and much weaker van der Waals interlayer forces, analogous to (0001) oriented graphite. In a previous paper, we examined the growth of a monolayer of graphene on Rh(111).[1] In this paper, we build on this, investigating the growth of stacked layers of graphene (up to four or five layers thick) and how some of their physical properties compare with monolayer graphene.

Graphene has many useful physical and electronic properties, and there is great interest in how these properties change in going from one to a few layers.[2−5] Free-standing single-layer graphene sheets exhibit a large thermal conductivity.[6] A large contribution to the thermal conductivity are low-energy flexural modes, where the motion is out-of-plane. This effect decreases with increasing numbers of layers, having largely disappeared by three-layer-thick graphene.[6] The thermal conductivity of supported monolayer graphene, though lower than free-standing, is still high.[7] He scattering is a nondestructive method of probing surface properties, both the structure[8] and vibrational spectrum, and is most sensitive to phonons polarized perpendicular to the surface plane.[9]

Monolayer graphene is grown on metal surfaces by exposing them to a hydrocarbon at elevated temperatures.[10] On Rh(111), graphene forms a lattice-mismatched overlayer that is aligned along the symmetry directions of the substrate.[11,12] The lattice mismatch results in a superlattice structure that shows up in scanning tunneling microscopy[13] and elastic He diffraction.[1] With the proper conditions, only monolayer graphene grows. To grow a multilayer, the metal surface temperature is raised until carbon from hydrocarbon cracking on the metal surface is able to diffuse into the bulk. Slow cooling allows it to diffuse to the surface, and depending on how much is adsorbed, multilayers are grown.[14]

In this paper, we explore the conditions for this growth to occur on Rh(111), using a combination of angle-resolved elastic He diffraction and Auger electron spectroscopy (AES). Under proper conditions, it is possible to grow large terraces of well-ordered graphene, with thicknesses ranging from 1 to 4 layers. The surface layer is azimuthally aligned with the Rh(111) substrate, though the lattices have different periodicities. We made Debye−Waller measurements, where the surface temperature dependence of the elastic scattering is measured, the attenuation being due to increased inelastic scattering with increased phonon population. We also made some direct measurements of the surface phonons by directly measuring inelastic He scattering. The result of these measurements is that the greatest change in the surface

Received: July 28, 2016
Revised: October 5, 2016
Published: October 17, 2016

DOI: 10.1021/acs.jpcc.6b07598
J. Phys. Chem. C 2016, 120, 24158−24164

vibrational properties happens when going from one to two layers. They demonstrate how the properties of these thin layered materials can be controlled by varying the number of layers.

EXPERIMENTAL SECTION

The apparatus was the same as that used for the growth of monolayer graphene on Rh(111).[1] The experimental apparatus consisted of an ultrahigh vacuum (UHV) chamber with a base pressure of ~2 × 10^{-10} Torr. Two different molecular beams, one for dosing and one for He scattering, were produced in a separate chamber connected to the UHV chamber through three regions of differential pumping. For measuring the He scattering, there is an electron bombardment ionizer and a double-differentially pumped quadrupole mass spectrometer, which can be moved in an arc around the position of the target, with a full width at half-maximum (fwhm) angular acceptance of ~1°. The plane of the arc defined by the detector motion is then the scattering plane within which the He is detected after colliding with the target. The target to ionizer distance is 14.45 cm. The UHV chamber also has an electron gun and single pass cylindrical-mirror electrostatic analyzer (CMA) for taking Auger electron spectra (AES).

The target was welded to a three axes mount that allowed for the independent adjustment of the incident angle of the molecular beam (θ_i, measured relative to the surface normal), the in-plane rotation of the target crystal (φ, the azimuth), and the tilt of the surface relative to the scattering plane. For the experiments described, the tilt was adjusted so that the surface plane was perpendicular to the scattering plane. The angle between the detector and the normal to the target surface is θ_f. The target was resistively heated and cryogenically cooled with either liquid nitrogen or liquid He. Surface temperature (T_S) was measured with a chromel−alumel thermocouple welded to the target crystal.

The target was a Rh single crystal, cut and polished to within better than 1° of the (111) face as determined by Laue X-ray backscattering. Cleaning was done by cycles of Ar^+ bombardment and O_2 exposure, both at 900 K. Annealing was done at ~1250 K, and cleanliness was determined with AES. After each cycle of cleaning and annealing, the He specular reflection was checked. After many cycles, the intensity of the reflection reached a constant value, and this value could be used to assess both surface cleanliness and surface order. For removing carbon overlayers, it was only necessary to expose the surface to O_2 at elevated temperatures. For multilayers, exposure to O_2 for about an hour at 1050 or 1100 K followed by a slow cool (10 K/min) to 1000 K with the crystal still exposed to the O_2 beam removed most of the carbon. Any oxygen could be removed by a 3 min anneal at ~1250 K. We think that this high temperature O_2 exposure is necessary because the O_2 does not readily stick and react with a carbon covered surface at lower temperatures. The high surface temperature allows some of the overlayer to diffuse into the crystal, exposing Rh where the O_2 can be dissociatively adsorbed and then react with the carbon. The slow cooling allows any absorbed carbon to diffuse to the surface and be reacted away.

Many graphene layers were grown during the course of these experiments, and it was found that the most sensitive method to determine whether all of the carbon was removed before a new layer was deposited was to use the He specular reflectivity of the Rh(111) surface. A small amount of adsorbed carbon led to a large attenuation of the signal, as explained by Poelsema and Comsa.[15]

Dosing was done with a neat beam of ethylene (Matheson, Research grade, >99.99% purity). As determined by the pressure rise in the UHV chamber, the pumping speed, and the diameter of the beam, we estimate that the flux was ~10^{14} cm^{-2} s^{-1}.

The He scattering was done with two different translational energies, accomplished by expanding high pressure He (several hundred psi) through a 10 μm pinhole. Beam velocities were determined by a time-of-flight (TOF) technique. The target could be lowered out of the beam path, and the detector rotated so the beam impinged directly on the ionizer. A rotating wheel with small slots mechanically chopped the beam, and by measuring the He signal in a series of small time bins of equal length, and knowing the distances, it was possible to determine the energy and energy spread of the beams. When cooled with liquid N_2, a typical beam had an average translational energy (E_i) of 19.3 meV with a $\Delta E/E_i$ = 0.03 fwhm. With the nozzle at ambient temperature, a typical beam had an E_i = 66 meV with a $\Delta E/E_i$ = 0.28 fwhm.

We did three types of He scattering experiments to characterize the surface properties. For diffraction and Debye−Waller measurements, we used a square-wave beam modulation, necessary to account for the detector background, which gives the total signal scattered into the final angle determined by the detector position. This was done with a rotating wheel in the second differential pumping region. For measuring phonons, we used standard time-of-flight (TOF) techniques, using a chopper disk with narrow slots, which allows us to measure the signal as a function of both flight time and θ_f.

RESULTS AND DISCUSSION

The first requirement was to determine how to grow the multilayers. At surface temperatures where there is a stable monolayer, there can be no further growth from the vacuum side, since the ethylene only decomposes on the metal and not the graphene surface.[16] Alternatively, the multilayer graphene can be grown from below, using carbon dissolved in the Rh.[14] Carbon has a moderate solubility in Rh at elevated temperatures.[17,18] Dong et al.[13] found the lower limit for dissolution to be 1053 K. We found that the surface temperature that reliably grew good monolayers was 1070 K.[1] However, dosing at T_S = 1170 K with C_2H_4 allowed carbon to be absorbed into the Rh. Though maybe not necessary, we first grew a monolayer, then heated the sample to 1170 K, and further exposed the crystal to C_2H_4. To allow the multilayer to form, we then cooled to 1000 K at 10 K/min. This slow cooling is necessary to allow the adsorbed carbon to diffuse to the surface.[14,18] The sample could then be cooled and checked for order and thickness with He diffraction and AES. If desired, we could reheat the sample to 1170 K and continue dosing to increase the coverage. Dosing times were between 15 min and an hour. It was also found that once cooled, it was a good idea to anneal for 20 min at T_S = 450 K, as evidenced by changes in the He diffraction spectra. At least in vacuum, the graphene could be stable for several days.

We had no explicit means of determining if the carbon overlayers grow layer-by-layer, though this seems a reasonable assumption considering that for (0001) oriented carbon sheets, there are much stronger in-plane sp^2 bonds than the bonds between the layers. Stacked sheets have been grown on many substrates such as SiC,[19,20] Cu,[21] and Ni.[22,23] Most pertinent to

DOI: 10.1021/acs.jpcc.6b07598
J. Phys. Chem. C 2016, 120, 24158−24164

our experiments, Liu et al.[14] grew multilayer graphene films with large terrace sizes on Rh foil.

To determine the thickness of the layers we grew, we used AES and assumed layer-by-layer growth.[24] Examples of the Auger spectra, which are the first derivative of the measured electron intensity, are shown in Figure 1. We used a Beers–

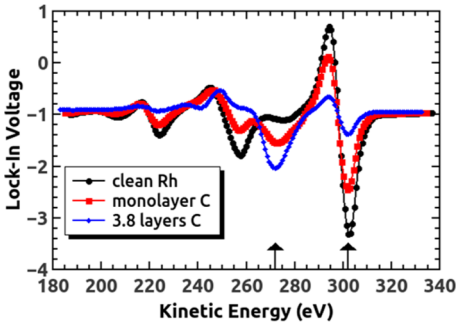

Figure 1. Auger electron spectra for various carbon coverages on Rh(111) taken with 1.5 eV incident electrons. Two arrows indicate the position of the largest feature for C (272) and Rh (302).

Lambert law type dependence of the Rh Auger signal to calibrate the number of layers

$$I_n = I_c \exp(-n/n_p) \quad (1)$$

where I_c is the peak-to-peak intensity for the clean Rh, I_n is the peak-to-peak intensity of the Rh with n layers of graphene, and n_p is the proportionality constant for a single layer of graphene. We can measure the Auger spectrum of the clean Rh(111). As discussed in the previous paper on single layer graphene,[1] with the proper surface temperature, the graphene growth stops at monolayer coverage. We infer that the monolayer coverage is complete, since any areas of exposed Rh(111) would lead to large specular scattering intensities for the He beam. From the He diffraction spectra, we know that the overlayer consists of large, well-ordered terraces. Since we can measure the Auger spectra for both clean and monolayer graphene-covered Rh(111), it is possible to determine n_p. Using the above procedure, we were also able to calibrate the coverage using the ratio of the carbon to Rh peak-to-peak intensities. This ratio was what was normally used for determining the number of graphene layers. It is important to note that the thickness measurements are only approximate, particularly since the model is not precise for partial layers. The value for coverage is only meant as an approximation; if a value of 2.3 layers is given, this means that the coverage is closer to 2 than 3 layers.

Figure 2 shows He diffraction spectra for three different thicknesses. The experimental conditions are the same (E_i = 19.3 meV, $[\bar{1}12]$ direction of the Rh surface, θ_i = 45°, and T_S = 200 K), the incident beam intensities were nearly the same, and so the results are directly comparable. The blue arrows indicate the position of the diffraction feature expected for the graphite lattice; the other peaks are due to the moiré pattern from the misfit between the graphene and the underlying Rh(111) surface.[1,25] Even up to 4 layers, the surface shows some corrugation due to this misfit. A second observation is that the specular and (11) graphite elastic diffraction peaks are larger for multilayer than monolayer graphene. This is probably due to a smaller misfit corrugation; there is less elastic scattering into the features corresponding to the moiré pattern. A further observation is that there is a large, broad feature under the

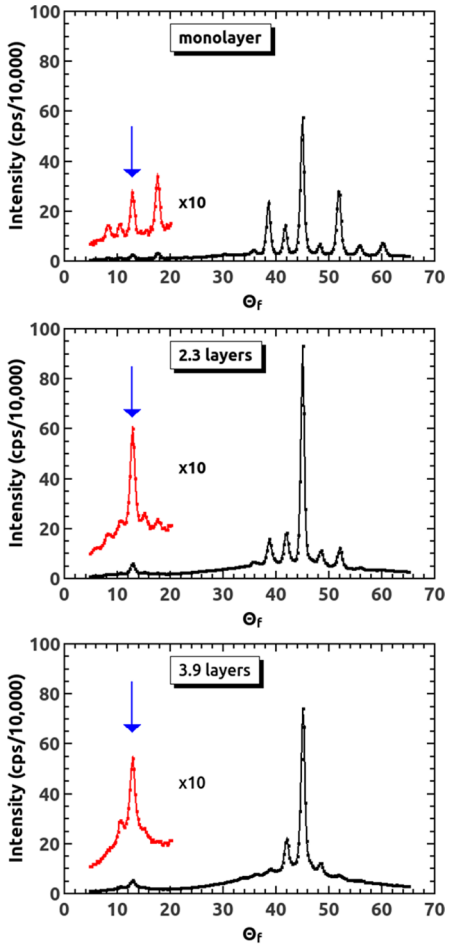

Figure 2. He diffraction spectra taken at θ_i for three different carbon coverages, with θ_i = 45°, T_S = 200 K, and E_i = 19.3 meV, along the $[\bar{1}12]$ direction. Blue arrows indicates the position where the (11) diffraction peak due to the graphite periodicity occurs.

specular peak that has a greater intensity for multilayer than monolayer graphene. As will be shown below, this is larger due to a greater amount of inelastic scattering. The angular widths of the diffraction peaks also contains information about the coherence length of the surface, i.e., terrace sizes.[26] The specular feature is particularly good, since it has no dispersion due to the energy spread of the incident He beam. Within our experimental error, the angular width of the incident beam and the specular reflection of both monolayer and multilayer graphene are the same. This indicates that the terrace widths are greater than ~200 Å in size.

We could also monitor the graphite diffraction feature as a function of the azimuth. It rapidly disappears if φ is changed from the $[\bar{1}12]$ of the Rh(111) substrate. This indicates that at least the top layer of the graphene is aligned to within 1° of the substrate symmetry direction, even for four layers of graphene. We cannot say whether the thicker layers have the ABAB packing expected for the (0001) oriented graphite.

Thermal vibrations of the surface lead to the attenuation of the elastic features: the Debye–Waller factor.[27,28] An example of this attenuation for monolayer graphene is shown in Figure 3. A simple model is given by

$$I(T_S) = I_0 \exp(-2W(T_S)) \quad (2)$$

DOI: 10.1021/acs.jpcc.6b07598
J. Phys. Chem. C 2016, 120, 24158–24164

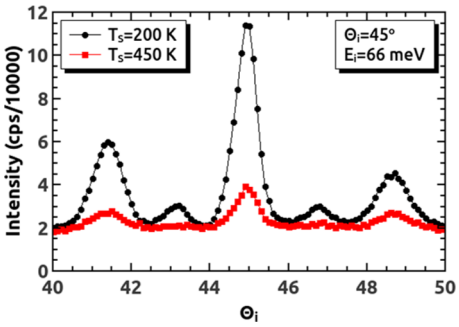

Figure 3. A comparison of He diffraction spectra at two different surface temperatures for monolayer graphene.

where $I(T_S)$ is the intensity of the elastic feature as a function of surface temperature. Figure 4 shows a plot of $\ln(I)$ for the

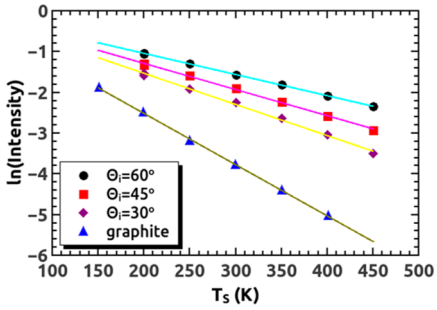

Figure 4. Examples of plots of $\ln(I)$ vs T_S for the specular reflection of 66 meV He from monolayer graphene at the indicated angles. The graphite results are from Oh et al.,[31] with $\theta_i = 45°$ and $E_i = 63$ meV. The data have been scaled so that $I_0 = 1$ (see text).

specular reflection at different θ_i vs T_S for monolayer graphene, using a 66 meV He beam and scaled so that $I_0 = 1$. The results are well fit with a straight line, with slope = $-2W$. Table 1 gives

Table 1. Values for the Slope of $\ln(I)$ vs T_S for the Specular Reflection of MLG, with an Incident Beam Energy of 66 meV and Three Different Angles[a]

θ_i (deg)	$2W$ (K^{-1})	95% confidence interval
30	0.007 68	±0.001 05
45	0.006 88	±0.000 86
60	0.005 93	±0.001 02

[a]This is the average for three different monolayers. For comparison, $2W = 0.012\,57$ K^{-1} for graphite with $E_i = 63$ meV and $\theta_i = 45°$.[31]

these values. Assuming a Debye model for the lattice vibrations, and including the Beeby correction,[29] an expression can be derived for the specular reflection:[28]

$$W(T_S) = 12m(E_i \cos^2 \theta_i + D)T_S/Mk_B\Theta_D^2 \quad (3)$$

where m is the He mass, M is the effective mass of the surface region with which the He interacts, D is the He–surface interaction potential well depth, k_B is Boltzmann's constant, and Θ_D is the Debye temperature. For D, we used 15.7 meV, the value from Boato et al.[30] for graphite. One problem with this model is that the He may interact with more than one surface atom, and so M is not necessarily the mass of a single surface atom. However, for the purposes of comparison with other results, M was set at the mass of a carbon for the derivation of Θ_D using eq 3. For the results listed in Table 1, this give values for Θ_D of 888 K at $\theta_i = 60°$, 811 K at $\theta_i = 45°$, and 710 K at $\theta_i = 30°$. The error bars do not overlap, and so we suspect that the difference in Θ_D at different angles is due to deficiencies in the model.

Also shown in Figure 4 are the results for graphite from Oh et al.[31] They get a value for Θ_D of 590 K for a 63 meV He beam incident at $\theta_i = 45°$, in reasonable agreement with Boato et al.,[30] who calculated a value of 530 K. From a comparison of these numbers, and an examination of the curves in Figure 4, it is apparent that the monolayer graphene supported on Rh(111) is appreciably stiffer than graphite. This result is qualitatively in agreement with the results of Politano et al.[32] for monolayer graphene grown on Ru(0001) (Θ_D = 1045 K) and for multilayer graphene grown on Ni(111) (Θ_D = 784 K).[33]

When we tried a Debye–Waller measurement for multilayer graphene with a 66 meV beam, we found the same difficulties that Oh et al.[31] found with graphite: the specular intensity rapidly fell with temperature, and there was a large inelastic background. This made an accurate measurement of the intensities difficult. In order to ameliorate this problem, we tried the Debye–Waller measurements using a 19.3 meV He beam. Some results for the specular intensity of monolayer and 2.3 layer graphene at $\theta_i = 45°$ are shown in Figure 5. The

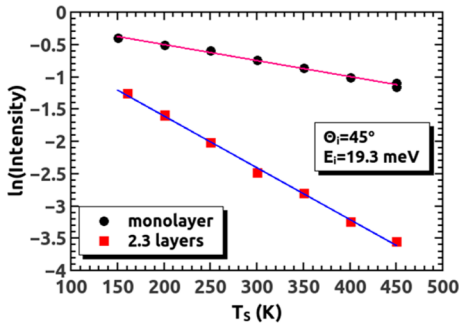

Figure 5. Comparison of the Debye–Waller attenuation of 1 and ~2 layer graphene for the specular reflection with 19.3 meV He. The data have been scaled so that $I_0 = 1$ (see text).

Debye–Waller exponent $2W = 0.002\,48$ K^{-1} for the monolayer and $0.008\,02$ K^{-1} for the 2.3 layer film, giving values for Θ_D from eq 3 of 974 K for monolayer graphene and 542 K for the 2.3 layer graphene. The temperature dependence for the specular He scattering intensity from multilayer graphene was experimentally identical for thicknesses between 2.2 and 4 layers. Though the model for the Debye–Waller attenuation may not be a perfect representation, it is important to note that the value of Θ_D for the 2.3 layer graphene is close to that found for graphite by Oh et al.[31] (590 K) and Boato et al.[30] (530 K). Vibrationally, the surface of two carbon layers is similar to graphite.

Figure 6 shows shows examples of TOF spectra for monolayer and four layer graphene along the $[\bar{1}12]$ direction. The black arrow at 370 ms indicates the position of the elastic He scattering. For these overlayers, this is a mixture of both scattering from defects and elastic diffraction. The experimental conditions are the same, so the results are directly comparable. The two colored arrows indicate the positions of the principle inelastic features, corresponding to phonon creation. It is clear that both the intensity and position for the two different surfaces are much different.

DOI: 10.1021/acs.jpcc.6b07598
J. Phys. Chem. C 2016, 120, 24158–24164

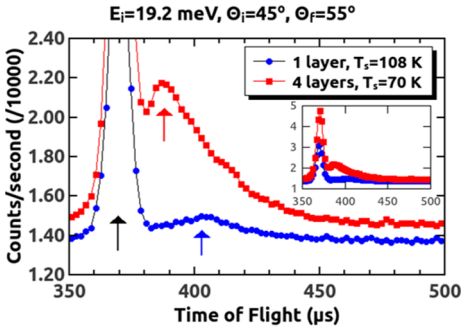

Figure 6. TOF spectra for monolayer and four layer graphene measured for the same experimental conditions. Black arrow indicates the position of the elastic feature; the colored arrows indicate the flight times used to calculate the phonon energies shown in Figure 7. The inset has the *y*-axis rescaled to show the full elastic feature.

We measured inelastic scattering for surface temperatures from 70 to 200 K, for both the monolayer and for multilayers between 2.6 and 5 layers thick. The results are summarized in the top panel of Figure 7, in a reduced surface Brillouin zone

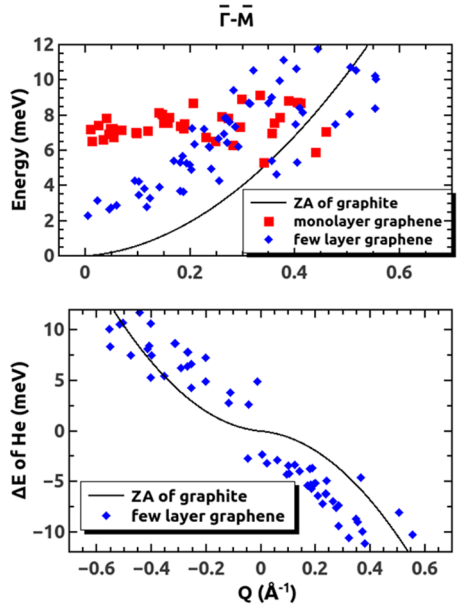

Figure 7. The top panel shows the absolute values of the measured phonon energies versus the absolute values of the parallel momentum exchange for both the monolayer and a few layers near the zone center. The multilayers varied between 2.6 and 4.6 layers thick. The bottom panel shows the measured dispersion relations for the multilayers (points) and the ZA mode of graphite (line).[34]

plot. The inelastic features are rather broad, probably not exclusively single phonon, but we used the peak maximum to calculate the phonon energy. The black line is the ZA acoustic mode of graphite.[34] The first observation is that near the zone center this perpendicularly polarized ZA mode does not go to zero, but an asymptotic value of ∼7 meV. This behavior is seen for monolayer graphene on Ni(111)[35] and Cu foil,[36] though not for Ru(0001).[37] This is due to the graphene−substrate interaction, and the frequency is a measure of the strength of that interaction.[35,38] For multilayers, the frequency more closely follows the graphite ZA branch. However, it does not go to 0 at the zone center. For graphene of N layers, the low lying acoustic mode splits into an acoustic mode and $N - 1$ low-frequency optical modes.[39,40] It is tempting to assign our observations to the inelastic features being an unresolved combination of these modes. However, the splitting is probably too large for this to be the explanation. Notice that the blue multilayer points seem to follow two arcs around the graphite ZA mode. Because of the kinematics of the He scattering, we principally observed phonon creation at $+\Delta Q$ and phonon annihilation at $-\Delta Q$. At $-\Delta Q$, the measured values were above the ZA value, and at $+\Delta Q$, they were below the ZA values. It is evident from the widths of the inelastic features that we are not resolving single phonons, so the peak maxima may be systematically varying from the true phonon energy for the mode. However, we can say that there is a definite difference between the low-energy, *z*-polarized modes of monolayer and multilayer graphene, and the change occurs rather abruptly over a small number of additional layers. This is in agreement with the Debye−Waller measurements, which show that the monolayer graphene surface is much stiffer than either a few layers or the surface of graphite.

CONCLUSIONS

As a continuation of our paper about supported monolayer graphene grown on Rh(111),[1] we looked at the growth of multilayer graphene and how some of its properties compare with the monolayer. The growth of multilayers is bottom up rather than top down; the hydrocarbons that normally supply the carbon for graphene growth do not decompose on the surface of graphene, so the Rh surface must be heated to temperatures where carbon can be absorbed. The Rh is then slowly cooled, allowing the carbon to diffuse to the surface. By varying the dosing time at the elevated temperature, multilayers of a varying number of layers can be produced. The thickness was determined by Auger electron spectroscopy and the surface ordering by He scattering. Monolayer graphene forms a lattice-mismatched but azimuthally aligned overlayer on Rh(111). Because of the lattice mismatch, the position of the carbon atoms with respect to the atoms of the Rh(111) surface slowly varies, leading to a superlattice structure, which shows up as the moiré pattern in diffraction experiments. The surface of the multilayers is also azimuthally aligned with the Rh(111) surface. Though attenuated, there is some remnant of the superlattice structure in the diffraction spectra at least up to four layers.

Another set of experiments involved measuring the attenuation of the elastic scattering as a function of surface temperature. This Debye−Waller factor is measure of the population of low-energy phonon modes; as the temperature increases and these modes become increasingly populated, there is increased inelastic scattering and thus a diminution of the elastic scattering intensities. The result was that the supported monolayer graphene is much "stiffer" (a higher Debye temperature) than even ∼2 layers.

The low-energy perpendicularly polarized phonon modes near the center of the Brillouin zone were measured with time- and angle-resolved inelastic He scattering. Unlike the graphite ZA acoustic mode, which goes to zero frequency at the zone center, the monolayer has a mode that is a nearly constant 7 meV near the zone center due to the graphene−rhodium interaction. The multilayer graphene scattering much more closely resembles that expected for the ZA mode of graphite. For the low-lying phonons with some degree of polarization perpendicular to the surface, there is a real difference between the surface dynamical properties as one transitions between a supported two-dimensional monolayer to three-dimensional

DOI: 10.1021/acs.jpcc.6b07598
J. Phys. Chem. C 2016, 120, 24158−24164

films consisting of only a few atomic layers. These findings add important information on how the properties of supported graphene films evolve with dimensional crossover from 2D to 3D systems and in particular demonstrate how thickness control on the scale of atomic dimensions can be used to achieve desired properties in thin 2D materials.

AUTHOR INFORMATION

Corresponding Author

*E-mail s-sibener@uchicago.edu; Tel 773-702-7193 (S.J.S.).

Notes

The authors declare no competing financial interest.

ACKNOWLEDGMENTS

This work was supported by the NSF-Materials Research Science and Engineering Center at The University of Chicago, Grant NSF-DMR-14-20709. Support was also provided by the Air Force Office of Scientific Research, Grant FA9550-15-1-0428.

REFERENCES

(1) Gibson, K. D.; Sibener, S. J. Helium Atom Scattering from Graphene Grown on Rh(111). *J. Phys. Chem. C* **2014**, *118*, 29077−29083.

(2) Chen, S.; Cai, W.; Piner, R. D.; Suk, J. W.; Wu, Y.; Ren, Y.; Kang, J.; Ruoff, R. S. Synthesis and Characterization of Large-Area Graphene and Graphite Films on Commercial Cu-Ni Alloy Foils. *Nano Lett.* **2011**, *11*, 3519−3525.

(3) Faugeras, C.; Nerriere, A.; Potemski, M.; Mahmood, A.; Dujardin, E.; Berger, C.; de Heer, W. A. Few-Layer Graphene on SiC, Pyrolitic Graphite, and Graphene: A Raman Scattering Study. *Appl. Phys. Lett.* **2008**, *92*, 011914.

(4) Falkovsky, L. A.; Pershoguba, S. S. Optical Far-Infrared Properties of a Graphene Monolayer and Multilayer. *Phys. Rev. B: Condens. Matter Mater. Phys.* **2007**, *76*, 153410.

(5) Yan, Z.; Nika, D. L.; Balandin, A. A. Thermal Properties of Graphene and Few-Layer Graphene: Applications in Electronics. *IET Circ. Devices Syst.* **2015**, *9*, 4−12.

(6) Lindsay, L.; Broido, D. A.; Mingo, N. Flexural Phonons and Thermal Transport in Multilayer Graphene and Graphite. *Phys. Rev. B: Condens. Matter Mater. Phys.* **2011**, *83*, 235428.

(7) Seol, J. H.; Jo, I.; Moore, A. L.; Lindsay, L.; Aitken, Z. H.; Pettes, M. T.; Li, X.; Yao, Z.; Huang, R.; Broido, D.; et al. Two-Dimensional Phonon Transport in Supported Graphene. *Science* **2010**, *328*, 213−216.

(8) Engel, T.; Rieder, K. H. Structural Studies of Surfaces with Atomic and Molecular Beam Diffraction. In *Structural Studies of Surfaces*; Springer Tracts in Modern Physics; Springer-Verlag: Berlin, 1982; Vol. *91*.

(9) Skofronick, J. G.; Toennies, J. P. Helium Scattering Studies of the Surface Phonons. In *Surface Properties of Layered Structures*; Physics and Chemistry of Materials with Low-Dimensional Structures; Kluwer Academic Publishers: 1992; pp 151−218.

(10) Batzill, M. The Surface Science of Graphene: Metal Interfaces, CVD Synthesis, Nanoribbons, Chemical Modifications, and Defects. *Surf. Sci. Rep.* **2012**, *67*, 83−115.

(11) Preobrajenski, A. B.; Ng, M. L.; Vinogradov, A. S.; Mårtensson, N. Controlling Graphene Corrugation on Lattice-Mismatched Substrates. *Phys. Rev. B: Condens. Matter Mater. Phys.* **2008**, *78*, 073401.

(12) Wang, B.; Caffio, M.; Bromley, C.; Früchtl, H.; Schaub, R. Coupling Epitaxy, Chemical Bonding, and Work Function at the Local Scale in Transition Metal-Supported Graphene. *ACS Nano* **2010**, *4*, 5773−5782.

(13) Dong, G. C.; van Baarle, D. W.; Rost, M. J.; Frenken, J. W. M. Graphene Formation on Metal Surfaces Investigated by in-Situ Scanning Tunneling Microscopy. *New J. Phys.* **2012**, *14*, 053033.

(14) Liu, M.; Zhang, Y.; Chen, Y.; Gao, Y.; Gao, T.; Ma, D.; Ji, Q.; Zhang, Y.; Li, C.; Liu, Z. Thinning Segregated Graphene Layers on High Carbon Solubility Substrates of Rhodium Foils by Tuning the Quenching Process. *ACS Nano* **2012**, *6*, 10581−10589.

(15) Poelsema, B.; Comsa, G. *Scattering of Thermal Energy Atoms from Disordered Surfaces*; Springer Tracts in Modern Physics; Springer-Verlag: Berlin, 1989.

(16) Loginova, E.; Bartelt, N. C.; Feibelman, P. J.; McCarty, K. F. Factors Influencing Graphene Growth on Metal Surfaces. *New J. Phys.* **2009**, *11*, 063046.

(17) Arnoult, W. J.; McLellan, R. B. The Solubility of Carbon in Rhodium Ruthenium, Iridium and Rhenium. *Scr. Metall.* **1972**, *6*, 1013−1018.

(18) Rut'kov, E.; Kuz'michev, A.; Gall', N. Carbon Interaction with Rhodium Surface: Adsorption, Dissolution, Segregation, Growth of Graphene Layers. *Phys. Solid State* **2011**, *53*, 1092−1098.

(19) Varchon, F.; Mallet, P.; Magaud, L.; Veuillen, J.-Y. Rotational Disorder in Few-Layer Graphene Films on 6H-SiC(000−1): A Scanning Tunneling Microscopy Study. *Phys. Rev. B: Condens. Matter Mater. Phys.* **2008**, *77*, 165415.

(20) Lauffer, P.; Emtsev, K. V.; Graupner, R.; Seyller, T.; Ley, L.; Reshanov, S. A.; Weber, H. B. Atomic and Electronic Structure of Few-Layer Graphene on SiC(0001) Studied with Scanning Tunneling Microscopy and Spectroscopy. *Phys. Rev. B: Condens. Matter Mater. Phys.* **2008**, *77*, 155426.

(21) Fallahazad, B.; Hao, Y.; Lee, K.; Kim, S.; Ruoff, R. S.; Tutuc, E. Quantum Hall Effect in Bernal Stacked and Twisted Bilayer Graphene Grown on Cu by Chemical Vapor Deposition. *Phys. Rev. B: Condens. Matter Mater. Phys.* **2012**, *85*, 201408.

(22) Reina, A.; Jia, X.; Ho, J.; Nezich, D.; Son, H.; Bulovic, V.; Dresselhaus, M. S.; Kong, J. Large Area, Few-Layer Graphene Films on Arbitrary Substrates by Chemical Vapor Deposition. *Nano Lett.* **2009**, *9*, 30−35.

(23) Reina, A.; Thiele, S.; Jia, X.; Bhaviripudi, S.; Dresselhaus, M. S.; Schaefer, J. A.; Kong, J. Growth of Large-Area Single- and Bi-Layer Graphene by Controlled Carbon Precipitation on Polycrystalline Ni Surfaces. *Nano Res.* **2009**, *2*, 509−516.

(24) Jackson, D. C.; Gallon, T. E.; Chambers, A. A Model for the Auger Electron Spectroscopy of Systems Exhibiting Layer Growth, and Its Application to the Deposition of Silver on Nickel. *Surf. Sci.* **1973**, *36*, 381−394.

(25) Sicot, M.; Leicht, P.; Zusan, A.; Bouvron, S.; Zander, O.; Weser, M.; Dedkov, Y. S.; Horn, K.; Fonin, M. Size-Selected Epitaxial Nanoislands Underneath Graphene Moiré on Rh(111). *ACS Nano* **2012**, *6*, 151−158.

(26) Gibson, K. D.; Cerjan, C.; Light, J. C.; Sibener, S. J. Elastic Helium Scattering Studies of Ordered Overlayers of Ar, Kr, and Xe Physisorbed on Ag(111). *J. Chem. Phys.* **1988**, *88*, 7911.

(27) Goodman, F. O. Determination of Characteristic Surface Vibration Temperatures by Molecular Beam Scattering. *Surf. Sci.* **1974**, *46*, 118−128.

(28) Farias, D.; Rieder, K.-H. Atomic Beam Diffraction from Solid Surfaces. *Rep. Prog. Phys.* **1998**, *61*, 1575−1664.

(29) Beeby, J. L. The Scattering of Helium Atoms from Surfaces. *J. Phys. C: Solid State Phys.* **1971**, *4*, L359.

(30) Boato, G.; Cantini, P.; Salvo, C.; Tatarek, R.; Terreni, S. Atomic Vibrations at the (0001) Graphite Surface Studied by He Atom Scattering. *Surf. Sci.* **1982**, *114*, 485−497.

(31) Oh, J. P.; Kondo, T.; Hatake, D.; Nakamura, J. Elastic and Inelastic Scattering Components in the Angular Intensity Distribution of He Scattered from Graphite. *Surf. Sci.* **2009**, *603*, 895−900.

(32) Politano, A.; Borca, B.; Minniti, M.; Hinarejos, J. J.; Vázquez de Parga, A. L.; Farías, D.; Miranda, R. Helium Reflectivity and Debye Temperature of Graphene Grown Epitaxially on Ru(0001). *Phys. Rev. B: Condens. Matter Mater. Phys.* **2011**, *84*, 35450.

DOI: 10.1021/acs.jpcc.6b07598
J. Phys. Chem. C 2016, 120, 24158−24164

(33) Tamtögl, A.; Bahn, E.; Zhu, J.; Fouquet, P.; Ellis, J.; Allison, W. Graphene on Ni(111): Electronic Corrugation and Dynamics from Helium Atom Scattering. *J. Phys. Chem. C* **2015**, *119*, 25983−25990.
(34) Mohr, M.; Maultzsch, J.; Dobardžić, E.; Reich, S.; Milošević, I.; Damnjanović, M.; Bosak, A.; Krisch, M.; Thomsen, C. Phonon Dispersion of Graphite by Inelastic X-Ray Scattering. *Phys. Rev. B: Condens. Matter Mater. Phys.* **2007**, *76*, 35439.
(35) Aizawa, T.; Souda, R.; Ishizawa, Y.; Hirano, H.; Yamada, T.; Tanaka, K.; Oshima, C. Phonon Dispersion in Monolayer Graphite Formed on Ni(111) and Ni(001). *Surf. Sci.* **1990**, *237*, 194−202.
(36) Al Taleb, A.; Yu, H. K.; Anemone, G.; Farias, D.; Wodtke, A. M. Helium Diffraction and Acoustic Phonons of Graphene Grown on Copper Foil. *Carbon* **2015**, *95*, 731−737.
(37) Maccariello, D.; Campi, D.; Al Taleb, A.; Benedek, G.; Farias, D.; Bernasconi, M.; Miranda, R. Low-Energy Excitations of Graphene on Ru(0001). *Carbon* **2015**, *93*, 1−10.
(38) Chen, L.; Huang, Z.; Kumar, S. Phonon Transmission and Thermal Conductance across graphene/Cu Interface. *Appl. Phys. Lett.* **2013**, *103*, 123110.
(39) Michel, K. H.; Verberck, B. Theory of the Evolution of Phonon Spectra and Elastic Constants from Graphene to Graphite. *Phys. Rev. B: Condens. Matter Mater. Phys.* **2008**, *78*, 85424.
(40) Yan, J.-A.; Ruan, W. Y.; Chou, M. Y. Phonon Dispersions and Vibrational Properties of Monolayer, Bilayer, and Trilayer Graphene: Density-Functional Perturbation Theory. *Phys. Rev. B: Condens. Matter Mater. Phys.* **2008**, *77*, 125401.

DOI: 10.1021/acs.jpcc.6b07598
J. Phys. Chem. C 2016, 120, 24158−24164